

Nonlinear theory of the slow-wave cyclotron amplifier

A. K. Ganguly and S. Ahn

Naval Research Laboratory, Washington, D.C. 20375

(Received 7 March 1990)

We have developed a three-dimensional nonlinear theory for the slow-wave cyclotron instability in a dielectrically loaded waveguide. The efficiency, gain, and bandwidth of the amplifier are calculated from a self-consistent solution of a set of coupled nonlinear differential equations describing the growth of the electromagnetic field and the evolution of the electron trajectories. Calculations show that very broadband amplification with high efficiency is possible in the slow-wave region of the propagating waves. The instantaneous bandwidth (full width at half maximum) near saturation depends on the efficiency (η) of the amplifier. For a cold beam, the bandwidth $\Delta\omega/\omega \approx 6\%$ at $\eta \approx 40\%$, but $\Delta\omega/\omega$ increases to 30% if the amplifier is operated at an efficiency of 20%. The efficiency is very sensitive to the axial velocity spread of the beam since interaction occurs with waves having large propagation constants. The maximum efficiency drops from 48% to 10% as the velocity spread increases from 0% to 5% but the bandwidth shows a small increase.

I. INTRODUCTION

The instability of the waveguide modes interacting with a relativistic beam guided by an applied uniform magnetic field \mathbf{B}_0 may occur due to three different mechanisms, namely, cyclotron maser radiation^{1,2} (CMR), drift-induced instability,³ and Weibel instability.⁴ All the mechanisms depend on an anisotropic velocity distribution of the electrons. In each case the energy is extracted from the perpendicular motion of the beam through the interaction with the transverse electric field and radiation occurs near the Doppler-shifted electron cyclotron frequency or a harmonic. The bunching mechanisms, however, are different for the three interactions. The instability in CMR results from the azimuthal bunching of electrons due to the relativistic variation of their masses with energy. Weibel instability and the drift-induced instability, on the other hand, are nonrelativistic in nature. The drift-induced instability was used by Ono *et al.*³ to develop a new microwave source called peniotron. The drift motion⁵ of the electrons ($\langle \mathbf{E}_{\text{rf}} \rangle \times \mathbf{B}_0 / B_0^2$ drift) is set up by a finite time average of an rf electric field which is at right angles to the applied magnetic field \mathbf{B}_0 . The drift motion occurs in such a way that the electrons move into a stronger electric-field region during the decelerating phase in their orbits whereas they move into a weaker electric-field region during their accelerating phase. Weibel instability originates from the axial bunching of the electrons caused by the Lorentz force $\mathbf{v}_T \times \mathbf{B}_{\text{rf}}$ where \mathbf{v}_T is the velocity of electrons perpendicular to both \mathbf{B}_0 and \mathbf{B}_{rf} .

For large axisymmetric orbits where the guiding center radius ($R_0 \approx 0$) is much smaller than the Larmor radius (r_L), the amplifier based on the drift-induced instability has the potential for extremely high efficiency⁶ in excess of 70% but has a narrow bandwidth of about 5%. For off-axis electron motion in small orbits ($R_0 > r_L$), the $\langle \mathbf{E}_{\text{rf}} \rangle \times \mathbf{B}_0 / B_0^2$ drift is negligible and the CMR and

Weibel instability compete with each other. The azimuthal bunching in CMR predominates for waves with phase velocity (v_{ph}) greater than the speed of light in vacuum (c) while the axial bunching in Weibel interaction predominates⁷ if $v_{\text{ph}} < c$. The theoretical efficiency for the CMR in fast-wave-gyrotron traveling-wave amplifier⁸ (TWA) is near 45% with a small bandwidth of about 5%. The highest efficiency achieved so far in gyro-TWA experiment⁹ is 23% with an output power of 25 kW at 34.7 GHz and the bandwidth is about 1%. The bandwidth of a gyro-TWA can be increased by tapering¹⁰ the waveguide and the applied magnetic field but the efficiency is low and the device is prone to oscillation. An instantaneous bandwidth of 28% in the K_a band (28–40 GHz) has been observed in the small signal regime and the beam current is less than 0.3 A to avoid absolute instability. Slow-wave cyclotron amplifiers are expected to have the same efficiency as gyro-TWA but are capable of producing amplification over a wide bandwidth. In this paper we consider a particular slow-wave structure, namely, a dielectrically lined waveguide as the interaction medium. The group velocity of the propagating modes in this waveguide remains approximately constant over a wide frequency range. The beam can be made resonant with the waves in the broad frequency range by properly choosing the cyclotron frequency and the axial velocity of the electrons.

Theoretical work on slow-wave cyclotron amplifiers dealt with linear analyses of the growth rate of the instability in both the cylindrical¹¹ and the rectangular¹² waveguides showing large bandwidth ($\sim 50\%$) under small signal condition. Here, we perform a nonlinear analysis to study the evolution of the system through the linear regime of interaction to saturation and provide a realistic estimate of the interaction efficiency as well as the bandwidth for large signal operation. We treat wave propagation in a dielectrically loaded waveguide with rectangular cross section. The rectangular configuration

is better than the cylindrical configuration as a slow-wave cyclotron amplifier. In rectangular geometry, the rf field components can be described by a set of orthogonal TE and TM modes¹³ with the fundamental waveguide mode being TE_{10} in character. Thus single mode propagation and an efficient cyclotron interaction with the lowest waveguide mode are possible. In the cylindrical geometry, TE and TM modes are separable only for the azimuthally symmetric modes. Moreover, the fundamental mode is TM_{01} and the TE_{0n} or the TM_{0n} modes with different radial eigen-numbers (n) are not orthogonal. Thus, mode coupling is a serious problem even for the modes with no angular variation.

The nonlinear analysis involves the solution of a set of coupled differential equations which self-consistently describes the evolution of the trajectories of an ensemble of electrons as well as the growth of the electromagnetic field. Since we are interested in the amplifier configuration, only a single frequency needs to be considered. This permits an average over a wave period to be performed which eliminates the fast-time-scale phenomena from the formulation and includes only a beamlet of electrons which enters the interaction region within one wave period. The slow-time-scale formulation has been extensively used to study the nonlinear regime in many coherent radiation sources such as gyrotrons,^{8,14,15} free-electron lasers,^{16,17} and orbitrons.¹⁸

The paper is organized as follows. The general formulation is given in Sec. II. A description of the vacuum modes of a dielectrically lined waveguide is included in the section. The nonlinear differential equations governing the beam-wave interaction are also shown. The numerical solutions of the coupled equations are discussed in Sec. III for some specific cases. Conclusions are presented in Sec. IV.

II. MODEL AND FORMALISM

An end view of the configuration under consideration is shown in Fig. 1. An annular beam of electrons with the guiding centers uniformly distributed in a circle of radius R_0 and an electromagnetic wave of arbitrary input power are simultaneously injected at $z=0$ into a rectangular waveguide partially filled with a dielectric. The beam is guided along helical trajectories by a uniform magnetic field B_0 applied along the axis of the waveguide (z axis). The beam is initially monoenergetic but may have an axial velocity spread. The subsequent evolution of the beam is treated self-consistently. In Fig. 1 the widths of the waveguide along the x and y axes are denoted, respectively, by $2L_x$ and L_y . The origin of the coordinate system is taken on the axis of the waveguide and the unit vectors will be denoted by \hat{e}_x, \hat{e}_y , and \hat{e}_z . The region $0 < |x| < d$ is vacuum and the region $d < |x| < d + w = L_x$ is dielectric. The dielectric constants of the two regions will be denoted by ϵ_0 and ϵ , respectively. The two regions have the same permittivity μ_0 .

The self-consistent evolution of the electromagnetic field and the trajectories of an ensemble of electrons can be calculated from a simultaneous solution of the

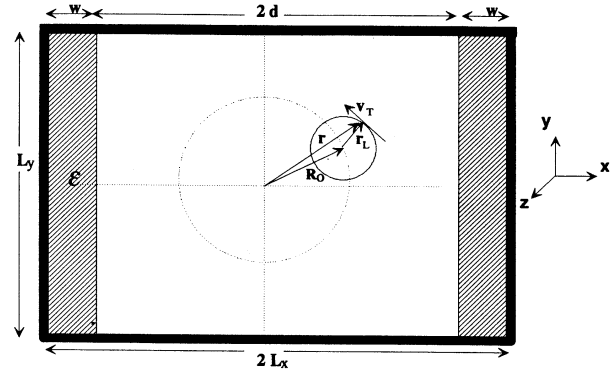


FIG. 1. End view of the dielectric loaded waveguide. Guiding centers of the electrons are uniformly distributed on a circle of radius R_0 .

Maxwell's equation and the Lorentz force equation

$$\nabla^2 \mathbf{E} - \mu_0 \epsilon \frac{\partial^2 \mathbf{E}}{\partial t^2} = \mu_0 \frac{\partial \mathbf{J}}{\partial t}, \quad (1)$$

$$\frac{d}{dt} (\gamma \mathbf{v}) = -\frac{e}{m_0} (\mathbf{v} \times \mathbf{B}_0) - \frac{e}{m_0} (\mathbf{E} + \mathbf{v} \times \mathbf{B}), \quad (2)$$

where \mathbf{B}_0 is the axial guide magnetic field, and \mathbf{E} and \mathbf{B} are the rf electric and magnetic fields, respectively. The rest mass of an electron is m_0 and e is the magnitude of its charge. The velocity of an electron and the current density are denoted, respectively, by \mathbf{v} and \mathbf{J} . The relativistic factor $\gamma = 1/[1 - (\mathbf{v} \cdot \mathbf{v})/c^2]^{1/2}$. The analysis will proceed under the following approximations: (a) an arbitrary number of TE_x modes¹³ (i.e., modes with the components of the electric field transverse with respect to the x axis) at a single frequency propagate in the waveguide, (b) the beam is tenuous, i.e., the plasma frequency (ω_p) is much smaller than the wave frequency (ω) such that the space-charge effects are negligible, and (c) the system is quasistatic in the sense that the electrons entering the interaction region at times t_0 separated by integral multiples of a wave period execute identical trajectories, i.e.,

$$\mathbf{v}(\mathbf{r}, t, t_0 + 2m\pi/\omega) = \mathbf{v}(\mathbf{r}, t, t_0).$$

With these assumptions, the set of coupled equations (1) and (2) can be solved in the slow-time-scale model¹⁴ where the fast cyclotron motion and the fast rf oscillations are averaged out. The inclusion of the multiple modes at the same frequency is based on the assumption that waves are coupled through the intermediary of the electrons and are not directly coupled. The individual source current for each mode is calculated from the integration of the electron orbit equations in the aggregate field of all modes. The only restriction is that all modes included in the calculation should be sufficiently close to resonance with the beam so that relative beam-wave phase

$$\Phi \approx (\omega - k_{zn} v_z - \Omega_0/\gamma) t$$

for each mode varies on a slow time scale. The axial wave vector for the n th mode is denoted by k_{zn} , the axial

velocity of the beam is v_z , and $\Omega_0 = eB_0/m_0$ is the cyclotron frequency.

We consider the uncoupled wave and beam modes before developing the slow-time-scale formulation. The modes of a dielectrically lined waveguide cannot be classified as either TE or TM with respect to the propagation direction along the z axis. However, they may be classified as TEx or TMx with respect to the x axis.¹³ These are also referred to as longitudinal section electric (LSE) and longitudinal section magnetic (LSM) modes, respectively. The modes may be divided into odd and even symmetries with respect to reflection at the yz plane. It will be shown in the Appendix that the even and odd modes couple, respectively, to the odd and even order cyclotron harmonics. Since our primary interest is the excitation of the fundamental cyclotron harmonic, we give detailed calculation for the even symmetry modes and mention the modifications necessary for the odd symmetry modes. For $L_y < 2L_x$, the fundamental mode is TEx₁₀ with even symmetry. We, therefore, restrict our attention to the TEx_{n0} modes.¹³

In the absence of an electron beam ($\mathbf{J}=0$), the nonzero field components of these modes are E_y , H_x , and H_z . The electric field for the TEx_{n0} modes is given from Eq. (1) by¹⁹

$$\mathbf{E} = \hat{\mathbf{e}}_y \frac{m_0 c^2}{e L_x} \operatorname{Re} \sum_{n=1}^{\infty} F_n Z_{n0}(x) \cos(\omega t - k_{z0} z), \quad (3)$$

where for even modes

$$Z_{n0}(x) = \begin{cases} \sin[\kappa'_n(L_x - |x|)] & d < |x| < L_x \\ \frac{\sin(\kappa'_n w)}{\cosh(\kappa_n d)} \cosh(\kappa_n x) & 0 < |x| < d \end{cases} \quad (4)$$

and for odd modes

$$Z_{n0}(x) = \begin{cases} \operatorname{sgn}(x) [\sin \kappa'_n(L_x - |x|)] & d < |x| < L_x \\ \frac{\sin(\kappa'_n w)}{\sinh(\kappa_n d)} \sinh(\kappa_n x) & 0 < |x| < d, \end{cases} \quad (5)$$

with

$$\kappa_n = (k_{z0}^2 - \mu_0 \epsilon_0 \omega^2)^{1/2}, \quad \kappa'_n = (\mu_0 \epsilon \omega^2 - k_{z0}^2)^{1/2}. \quad (6)$$

In Eq. (3), F_n is the wave amplitude, ω is the angular frequency, and k_{z0} is the unperturbed propagation constant. The rf magnetic-field components can be obtained for Maxwell's equation $\nabla \times \mathbf{E} = -\partial \mathbf{B} / \partial t$. By applying the relevant boundary conditions at $x=0, \pm d$, and $\pm L_x$, the unperturbed dispersion relation¹⁹ is given by

$$\begin{aligned} \kappa_n \tanh(\kappa_n d) + \kappa'_n \cot(\kappa'_n w) &= 0 \quad \text{for even modes} \\ \kappa_n \coth(\kappa_n d) + \kappa'_n \cot(\kappa'_n w) &= 0 \quad \text{for odd modes.} \end{aligned} \quad (7)$$

The subscript n refers to the n th root of Eq. (7). It can be easily verified that the functions $Z_{n0}(x)$ are orthogonal and we have

$$\int_{-L_x}^{L_x} \int_0^{L_y} Z_{n0}(x) Z_{n'0}(x) dx dy = \begin{cases} 0 & \text{for } n \neq n' \\ L_x^2 N_n & \text{for } n = n', \end{cases} \quad (8)$$

where the normalization constant N_n for the even modes is given by

$$N_n = \frac{L_y}{L_x} \left[\frac{d}{L_x} \frac{\sin^2(\kappa'_n w)}{\cosh^2(\kappa_n d)} \left[\frac{\sinh(2\kappa_n d)}{2\kappa_n d} + 1 \right] + \frac{w}{L_x} \left[1 - \frac{\sin(2\kappa'_n w)}{2\kappa'_n w} \right] \right], \quad (9)$$

while for the odd modes

$$N_n = \frac{L_y}{L_x} \left[\frac{d}{L_x} \frac{\sin^2(\kappa'_n w)}{\sinh^2(\kappa_n d)} \left[\frac{\sinh(2\kappa_n d)}{2\kappa_n d} - 1 \right] + \frac{w}{L_x} \left[1 - \frac{\sin(2\kappa'_n w)}{2\kappa'_n w} \right] \right]. \quad (10)$$

A typical dispersion curve and the field distribution for the fundamental TEx₁₀ mode are shown in Figs. 2(a) and 2(b), respectively. Fast-wave propagation occurs when $0 < k_{z0} < \sqrt{\mu_0 \epsilon_0 \omega}$ and slow-wave propagation exists for $\sqrt{\mu_0 \epsilon_0 \omega} < k_{z0} < \sqrt{\mu_0 \epsilon \omega}$. The transition occurs at $k_{z0} = k_s$ such that $\omega = ck_s$ where $c = \sqrt{1/\mu_0 \epsilon_0}$ is the speed of light in vacuum. From Eqs. (6)–(7), it can be shown that

$$k_s = \pi / [2w(\epsilon/\epsilon_0 - 1)^{1/2}].$$

For $k_{z0} < k_s$ we have $\omega > ck_{z0}$ (fast wave) and $\omega < ck_{z0}$ (slow wave) for $k_{z0} > k_s$. From Fig. 2(b), it is seen that for

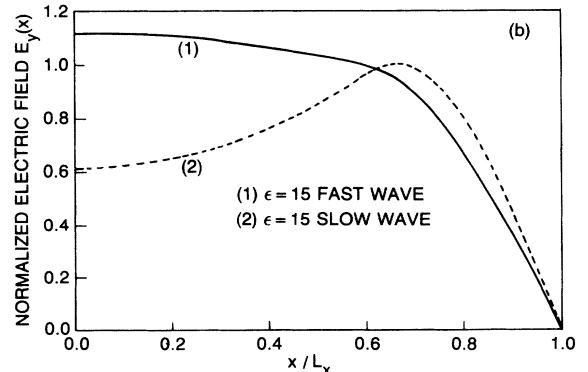
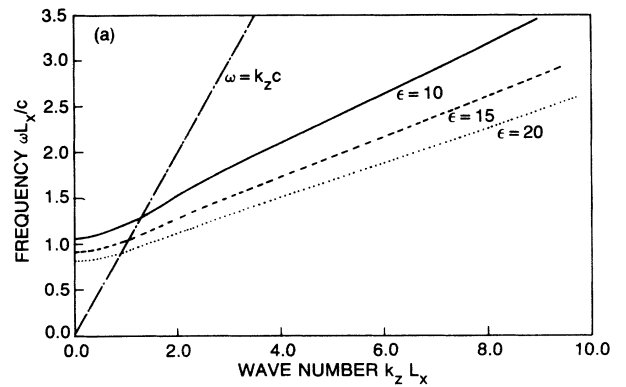


FIG. 2. (a) Dispersion relation for dielectric loaded waveguide of rectangular cross section. (b) E_y as a function of x .

fast waves the field is maximum on the axis while for slow waves the maximum occurs inside the dielectric. Hence, the beam should be placed close to the dielectric layer for strong interaction with the slow waves. In Eq. (3), κ_n is imaginary for the fast waves and Eqs. (2)–(5) should be used with the following substitution:

$$\begin{aligned} \kappa_n &\rightarrow i\kappa_n, \\ \cosh(\kappa_n x) &\rightarrow \cos(\kappa_n x), \end{aligned}$$

and $\sinh(\kappa_n x) \rightarrow i \sin(\kappa_n x)$.

When the beam is injected into the waveguide, we seek solutions of the form in Eq. (3) where the amplitude $F_n(z)$ and the wave vector $k_z(z)$ become slowly varying functions of z such that

$$\frac{d}{dz}[\ln F(z)] \ll k_z \quad \text{and} \quad \frac{d}{dz}(\ln k_z) \ll k_z. \quad (11)$$

The cutoff wave vectors κ_n and k'_n , however, are considered to be characteristics of the waveguide without the beam and remain constant throughout the course of the interaction. The rf field components in the presence of an electron beam can be written as

$$\mathbf{E} = \hat{\mathbf{e}}_y \frac{m_0 c^2}{eL_x} \sum_{n=1}^{\infty} F_n(z) Z_{n0}(x) \cos \alpha_n, \quad (12)$$

$$\begin{aligned} \mathbf{H} = & \frac{m_0 c^2}{\mu_0 \omega e L_x} \\ & \times \sum_{n=1}^{\infty} \left[\left(\frac{dF_n(z)}{dz} \sin \alpha_n - \frac{d\xi}{dz} F_n(z) \cos \alpha_n \right) Z_{n0}(x) \hat{\mathbf{e}}_x \right. \\ & \left. - F_n(z) \frac{dZ_{n0}(x)}{dx} (\sin \alpha_n) \hat{\mathbf{e}}_z \right], \quad (13) \end{aligned}$$

where

$$\alpha_n(z) = \omega t - \xi = \omega t - \int_0^z k_z(z') dz', \quad (14)$$

$$k_z = \frac{d\xi}{dz}. \quad (15)$$

We now consider the propagation of the electron beam. In the absence of the electromagnetic fields ($\mathbf{E} = \mathbf{0}$, $\mathbf{B} = \mathbf{0}$), the unperturbed orbits of the electrons from Eq. (2) may be written as

$$\mathbf{r}^{(0)} = (X_0^{(0)} + r_L^{(0)} \cos \Psi^{(0)}) \hat{\mathbf{e}}_x + (Y_0^{(0)} + r_L^{(0)} \sin \Psi^{(0)}) \hat{\mathbf{e}}_y + z \hat{\mathbf{e}}_z, \quad (16)$$

$$\mathbf{v}^{(0)} = -v_{T0} (\sin \Psi^{(0)}) \hat{\mathbf{e}}_x + v_{T0} (\cos \Psi^{(0)}) \hat{\mathbf{e}}_y + v_{z0} \hat{\mathbf{e}}_z, \quad (17)$$

where $\Psi^{(0)} = \Omega^{(0)} t$, $\Omega^{(0)} = \Omega_0 / \gamma_0 = eB_0 / \gamma_0 m_0$ is the relativistic cyclotron frequency, $v_{T0} = r_L^{(0)} \Omega_0 / \gamma_0$ and v_{z0} are the perpendicular and parallel components of electron velocity, $r_L^{(0)}$ is the Larmor radius and the guiding center coordinates are $(X_0^{(0)}, Y_0^{(0)})$.

In the presence of a signal, it is possible to obtain solutions¹⁴ of the form in Eqs. (16) and (17) where v_T , v_z , r_L , Ω , γ , X_0 , and Y_0 are allowed to vary slowly as functions of z satisfying the inequality conditions similar to those in

Eq. (11). Thus, we may write

$$\mathbf{r} = (X_0 + r_L \cos \Psi) \hat{\mathbf{e}}_x + (Y_0 + r_L \sin \Psi) \hat{\mathbf{e}}_y + z \hat{\mathbf{e}}_z, \quad (18)$$

$$\frac{d\mathbf{r}}{dt} = \mathbf{v} = -v_T (\sin \Psi) \hat{\mathbf{e}}_x + v_T (\cos \Psi) \hat{\mathbf{e}}_y + v_z \hat{\mathbf{e}}_z, \quad (19)$$

$$v_T = r_L \Omega = r_L \frac{\Omega_0}{\gamma}. \quad (20)$$

Equations (18) and (19) imply that the guiding center motion is determined by the equations

$$\frac{dX_0}{dt} + \frac{dr_L}{dt} \cos \Psi - r_L \left[\frac{d\Psi}{dt} - \Omega \right] \sin \Psi = 0, \quad (21)$$

$$\frac{dY_0}{dt} + \frac{dr_L}{dt} \sin \Psi + r_L \left[\frac{d\Psi}{dt} - \Omega \right] \cos \Psi = 0. \quad (22)$$

On substituting Eqs. (12)–(22) in Eqs. (1) and (2) and averaging the resulting equations over a wave period, the set of coupled nonlinear differential equations for the slow-time-scale variables can be derived by a procedure similar to that used for the fast-wave gyrotrons.^{8,15} The derivation is shown in the Appendix. Here we write the resulting equations in a normalized form which scales out the width of the waveguide, L_x . The dimensionless variables to be used are defined as follows: normalized length $\xi = z / L_x$, normalized wave vector $\chi = k_z L_x = L_x d\xi / dz$, normalized frequency $\bar{\omega} = \omega L_x / c$, normalized time $\tau = ct / L_x$, normalized velocity $\beta_{T,z} = v_{T,z} / c$, normalized electric field $F_n = eEL_x / m_0 c^2$, and normalized magnetic field $\bar{\Omega}_0 = \gamma \Omega = eBL_x / m_0 c$. Equations (A11) and (A12), describing the variation of the wave amplitude and the wave vector due to the interaction with the s th cyclotron harmonic, may be written in normalized form as

$$\begin{aligned} & \left[\frac{d^2}{d\xi^2} + \chi_0^2 - \chi^2 \right] F_n(z) \\ & = - \frac{2\bar{I}_0 \bar{\omega} \Theta_n}{N_n} \left\langle \frac{\beta_T}{|\beta_z|} \frac{\beta_{z0}}{\langle \beta_{z0} \rangle} I'_s(\kappa_n r_L) \right. \\ & \quad \left. \times \cosh(\kappa_n X_0) \sin \Phi \right\rangle, \quad (23) \end{aligned}$$

$$\begin{aligned} & 2\chi^{1/2} \frac{d}{d\xi} [\chi^{1/2} F_n(z)] \\ & = \frac{2\bar{I}_0 \bar{\omega} \Theta_n}{N_n} \left\langle \frac{\beta_T}{|\beta_z|} \frac{\beta_{z0}}{\langle \beta_{z0} \rangle} I'_s(\kappa_n r_L) \cosh(\kappa_n X_0) \cos \Phi \right\rangle, \quad (24) \end{aligned}$$

where $I'_s(a) = dI_s/da$,

$$\Phi = \omega(t - t_0) - \xi - s\Psi + \Psi_0$$

is the slowly varying phase difference between the beam and the wave, the normalized current $\bar{I}_0 = eI_0 / \epsilon_0 m_0 c^3$, and

$$\Theta_n = \begin{cases} \sin(\kappa'_n w) / \cosh(\kappa_n d) & \text{for even mode} \\ \sin(\kappa'_n w) / \sinh(\kappa_n d) & \text{for odd mode} \end{cases} \quad (25)$$

As shown in the Appendix, the cyclotron harmonic number s is odd when the resonant mode is of even symmetry and it is even for an odd symmetry mode.

Equations (A16)–(A18) for the phase Ψ and the components of the normalized momentum ($u_z = \gamma\beta_z$, $u_T = \gamma\beta_T$) of the electrons in their orbits take the dimensionless forms

$$\frac{du_T}{d\xi} = - \sum_n \Theta_n I'_s(\kappa_n r_L) \cosh(\kappa_n X_0) \times \left[\left[1 - \frac{\beta_z \chi}{\bar{\omega}} \right] \frac{F_n}{\beta_z} \cos\Phi + \frac{1}{\bar{\omega}} \frac{dF_n}{d\xi} \sin\Phi \right], \quad (26)$$

$$\frac{du_z}{d\xi} = - \sum_n \frac{u_T}{u_z} \Theta_n I'_s(\kappa_n r_L) \cosh(\kappa_n X_0) \times \left[\frac{\chi}{\bar{\omega}} F_n \cos\Phi - \frac{1}{\bar{\omega}} \frac{dF_n}{d\xi} \sin\Phi \right], \quad (27)$$

$$\frac{d\Psi}{d\xi} - \frac{\bar{\Omega}_0}{\gamma\beta_z} = - \sum_n \frac{\Theta_n s I_s(\kappa_n r_L)}{\bar{\omega} \kappa_n r_L u_T} \cosh(\kappa_n X_0) \times \left[\left[\bar{\omega} - \beta_z \chi + \frac{\kappa_n^2 r_L^2 \bar{\Omega}_0}{s\gamma} \right] \frac{F_n}{\beta_z} \sin\Phi - \frac{dF_n}{d\xi} \cos\Phi \right], \quad (28)$$

and

$$\frac{d\tau}{d\xi} = \frac{1}{\beta_z}. \quad (29)$$

Equations (26) and (27) can be combined to give the rate of change of energy of an electron,

$$\frac{d\gamma}{d\xi} = - \sum_n \frac{u_T}{u_z} \Theta_n I'_s(\kappa_n r_L) \cosh(\kappa_n X_0) F_n \cos\Phi. \quad (30)$$

The equations for the guiding center motion given by Eqs. (A19) and (A20) become in normalized form,

$$\frac{d\bar{X}_0}{d\xi} = \sum_n \frac{\Theta_n I_s(\kappa_n r_L)}{\bar{\Omega}_0} \sinh(\kappa_n X_0) \times \left[\left[\frac{\bar{\omega} - \chi\beta_z - s\bar{\Omega}}{\bar{\omega}} \right] \frac{F_n}{\beta_z} \cos\Phi + \frac{1}{\bar{\omega}} \frac{dF_n}{d\xi} \sin\Phi \right], \quad (31)$$

$$\frac{d\bar{Y}_0}{d\xi} = \sum_n \Theta_n I'_s(\kappa_n r_L) \sinh(\kappa_n X_0) \frac{\kappa_n r_L}{\gamma\bar{\omega}} \frac{F_n}{\beta_z} \sin\Phi, \quad (32)$$

where $\bar{X}_0 = X_0/L_x$ and $\bar{Y}_0 = Y_0/L_x$.

The power flow in the waveguide is calculated by integrating the axial component of the Poynting vector over the cross section of the guide:

$$P_{\text{out}} = \frac{1}{2} \text{Re} \int (\mathbf{E} \times \mathbf{H}^*) \cdot \hat{\mathbf{e}}_z dx dy = \frac{\epsilon_0 m_0^2 c^5}{2e^2} \sum_n N_n \frac{ck_z}{\omega} F_n^2. \quad (33)$$

The growth rate of the amplifier $\Gamma = (1/F_n)(dF_n/dz)$ can be calculated from Eq. (24) and its efficiency is given by $\eta = (P_{\text{out}} - P_{\text{in}})/V_0 I_0$, where V_0 is the beam voltage ($\gamma = 1 + eV_0/m_0 c^2$), I_0 is the current, and P_{in} is the input signal power. The summation over the mode index number (n) in Eqs. (26)–(33) includes only those modes at a given frequency for which $\Phi = \omega t - \xi - \Psi$ is small.

III. NUMERICAL RESULTS

The set of equations (23)–(33) are solved by specifying the initial conditions of the beam and the input signal. The initial conditions on the radiation field are chosen such that $dF_n/dz = 0$ and $k_z = d\xi/dz = k_{z0}$ at $z = 0$. The amplitude F_n at $z = 0$ is calculated from the input signal power using Eq. (33). The initial states of the electrons at $z = 0$ are chosen to model the injection of a monoenergetic beam with uniform distribution in phase and cross section, i.e., $\sigma_{\parallel}(\Psi_0) = 1$ for $0 \leq \Psi_0 \leq 2\pi$, and $\sigma_T(R_0, \Theta_0) = 1$ for $0 \leq \Theta_0 \leq 2\pi$, $R_{\text{min}} \leq R_0 \leq R_{\text{max}}$, where $R_0 = (X_0^2 + Y_0^2)^{1/2}$ and $\tan\Theta = Y_0/X_0$. Although the beam is monoenergetic, it may have an axial velocity spread and we assume that the initial distribution function is of the form

$$f_0(\mathbf{p}) \propto \exp[-(p_z - p_{z0})^2/2(\Delta p_z)^2] \times \delta(p_T^2 + p_z^2 - p_{T0}^2 - p_{z0}^2).$$

Only one experiment²⁰ has been reported for the slow-wave cyclotron amplifier. The experiment was performed at frequencies near 6 GHz in the TE₀₁ mode of a dielectric-loaded cylindrical waveguide operating with a 67.6-kV, 8-A beam having a high $\alpha \approx 5.0$ and a large velocity spread $\Delta v_z/v_{z0} > 5\%$. The dielectric constant used in the experiment is $\epsilon = 4.7\epsilon_0$ and the magnetic field $B_0 = 2.26$ kG. The observed instantaneous bandwidth is only 3.7% since the ‘‘grazing condition’’ (the beam line is tangential to the dispersion curve) required for large bandwidth was not accessible with the experimental parameters. The measured efficiency is also small because of the axial beam velocity spread. The calculations will show that the efficiency is very sensitive to $\Delta v_z/v_{z0}$. Since the experimental parameters were not favorable for high efficiency and large bandwidth amplifier, we show calculated results for parameters which are experimentally accessible.

The output power depends on a large number of beam and waveguide parameters. We will keep some of the parameters fixed and study the dependence of the efficiency and bandwidth on the other parameters. We choose the lowest waveguide mode ($n = 1$) and the fundamental cyclotron harmonic ($s = 1$) so that the interaction is efficient. From Eq. (24), it is seen that the growth rate is inversely proportional to the aspect ratio, $L_y/2L_x$, of the waveguide. We set $L_y/2 = d = 0.6L_x$ so that the aspect ratio is small but the dimensions are large enough for beam propagation without interception. We consider an infinitely thin beam to reduce the time of computation. The inclusion of a finite thickness beam is straightforward but requires more particles. We choose $R_0 = 0.05L_x$ so that $|R_0 + r_L| \approx 0.9d$ at the applied mag-

netic fields. The value of ϵ of the dielectric layer is an important parameter. The group velocity of the waves, $v_g = \partial\omega/\partial k_z$, should be nearly equal to v_z for grazing condition. For a fixed value of the velocity ratio $\alpha = v_T/v_z$, higher beam energy is required to maintain grazing condition with increase in v_g . The average slope of the $\omega - k_z$ curves (Fig. 2) in the slow-wave region increases with decrease in ϵ but the modes become more dispersive. A degradation of bandwidth and efficiency occurs at low as well as at high values of ϵ . For beam energies in the range 60 to 100 keV and $\alpha \sim 1.5$, high efficiency and large bandwidth are obtained with $\epsilon_r = \epsilon/\epsilon_0$ lying between 10 and 15. Some common materials with high dielectric constants and low loss tangents are alumina²¹ ($\epsilon_r = 9.5$, $\tan\delta = 0.0001$), sapphire²² ($\epsilon_r = 11.7$, $\tan\delta = 0.0001$), magnesium titanate²¹ ($\epsilon_r = 16.0$, $\tan\delta = 0.0002$), and lanthanum gallate²³ ($\epsilon_r = 24.3$, $\tan\delta = 0.0007$). These materials are used as substrates for very low loss-shielded or -unshielded microstrip transmission lines. Since the loss tangents are very small, we neglect propagation losses in the medium.

In the following figures we show the variation of the efficiency, gain, and bandwidth with γ , β_z , α , Ω_0 , and ϵ . A beam current $I_0 = 5$ A and an input signal power $P_{in} = 150$ W are used in all calculations. The results in Figs. 3–6 are calculated with $\epsilon/\epsilon_0 = 15$ and $\gamma = 1.12$ ($V_0 = 61.3$ kV). The cutoff frequency $\omega_{cut} = 0.913c/L_x$ and the group velocity of the slow waves $v_g = 0.232c$ for the waveguide parameters being used. The optimum efficiency and bandwidth are obtained with an applied magnetic field $\bar{\Omega}_0 = 0.924$ and $v_z = 0.24c$ ($\alpha = 1.588$). The output power as a function of the axial position is shown in Fig. 3 at two frequencies $f/f_{cut} = 1.24$ and 1.44 for which the saturation gain differs by about 3 dB. The lower frequency has a maximum efficiency $\eta_{max} = 48.5\%$ and maximum gain $G_{max} = 30$ dB. The interaction length required for saturation is $L_z = 85.2L_x$. The higher frequency saturates at a shorter interaction length $L_z = 41.6L_x$ with $\eta_{max} = 23.7\%$ and $G_{max} = 26.9$ dB. The normalized growth rates ($\Gamma L_x = L_x d \ln F_n / dz$) for the

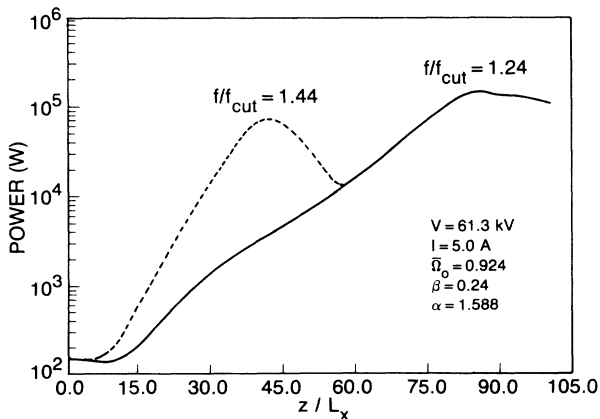


FIG. 3. Power in the waveguide as a function of axial position for two frequencies $f/f_{cut} = 1.24$ and 1.44 . Other parameters are $\gamma = 1.12$, $\beta_z = 0.24$, $\bar{\Omega}_0 = \gamma\Omega_0 = 0.924$, $\alpha = 1.588$, $\epsilon = 15\epsilon_0$, $\Delta v_z/v_z = 0$, $I_0 = 5$ A, $P_{in} = 150$ W, and $d = 0.6L_x$.

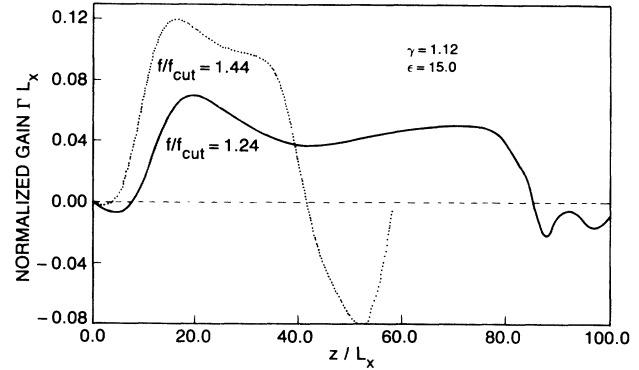


FIG. 4. Growth rate vs axial position for the same parameters as in Fig. 3.

two frequencies are shown in Fig. 4 as functions of z . The average normalized growth rates in the linear region are approximately 0.049 and 0.093 for the two frequencies.

The effect of a spread in the axial velocity of the electrons is shown in Fig. 5 where the efficiency is plotted as a function of frequency for different values of $\Delta v_z/v_z$. The efficiency of the slow-wave cyclotron amplifier is much more sensitive to the velocity spread than the fast-wave gyrotron since the propagation constant for the slow waves is larger. In Fig. 5 the maximum efficiency drops from 48.5% to 12.2% as $\Delta v_z/v_z$ is raised from 0 to 5%. The frequency for maximum efficiency increases with $\Delta v_z/v_z$. The results in Fig. 5 do not show the instantaneous bandwidth since the modes at different frequencies saturate at different axial positions.

The instantaneous bandwidth can be obtained from the η versus f curves plotted in Fig. 6. The 3-dB bandwidth ($\Delta\omega/\omega_0$) is the frequency range representing the full width at half maximum (FWHM) of the output power versus frequency curves. The center frequency of the band is denoted by ω_0 . If $P_{in} \ll P_{out}$, then the bandwidth is, also, given by the FWHM of the η versus f curves. The bandwidth, of course, depends on the peak power

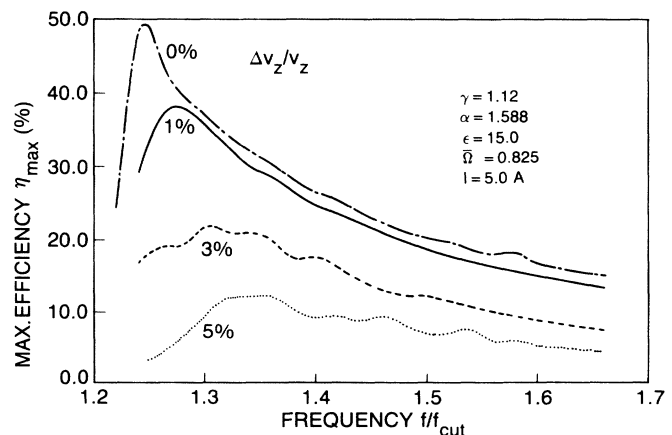


FIG. 5. Maximum efficiency vs frequency for different values of $\Delta v_z/v_z = 0.0, 0.01, 0.03$, and 0.05 . All other parameters are the same as in Fig. 3.

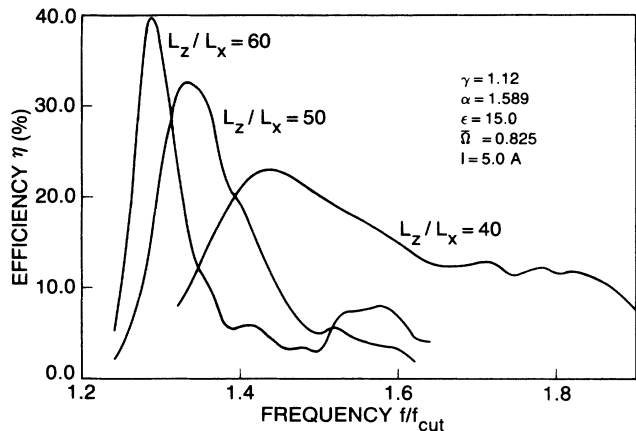


FIG. 6. Efficiency as a function of frequency for fixed interaction lengths $L_z/L_x=40, 50,$ and 60 with beam and waveguide parameters the same as in Fig. 5.

level at which $\Delta\omega/\omega$ is calculated. The three curves in Fig. 6 show that $\Delta\omega/\omega=31.4\%, 9.7\%,$ and $5.5\%,$ respectively, at peak efficiencies $\eta_p=23.0\%, 32.2\%,$ and $38.5\%.$ The corresponding values of the peak gain are 26.72, 28.15, and 28.96 dB with output power $P_{out}=70.5, 98.1,$ and 118.0 kW, respectively. The interaction lengths required are $L_z=40L_x, 50L_x,$ and $60L_x,$ respectively. The bandwidth increases to 40% if the gain is lowered to 20 dB but the efficiency is low ($\sim 5\%$). These results are in agreement with the linear theory.^{11,12}

In Fig. 7 we compare the bandwidth of the amplifier for two values of the dielectric constant, $\epsilon=10.0\epsilon_0$ and $15.0\epsilon_0,$ keeping the dimensions of the waveguide the same. The normalized cutoff frequencies for the two cases are 1.309 and 0.913, respectively, and the group velocities in the slow-wave regions are $v_g\approx 0.277c$ and $0.232c.$ To obtain grazing condition in both cases, we

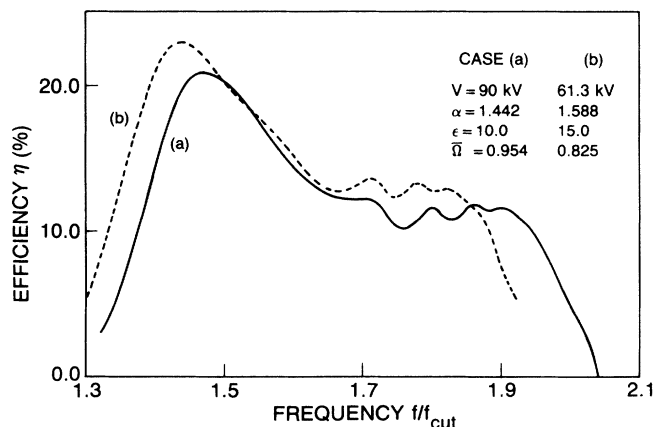


FIG. 7. Plot of efficiency as a function of frequency for two values of dielectric constant. (a) Solid curve: $\epsilon=10\epsilon_0, \beta_z=0.3, \alpha=1.442, \bar{\Omega}_0=\gamma\bar{\Omega}=1.122,$ and $V_0=90$ kV; (b) dashed curve: $\epsilon=15\epsilon_0, \beta_z=0.24, \alpha=1.588, \bar{\Omega}_0=\gamma\bar{\Omega}=0.924,$ and $V_0=61.3$ kV.

choose $\beta_z=0.3, \bar{\Omega}_0=1.122,$ and $V_0=90$ kV for the first case and $\beta_z=0.24, \bar{\Omega}_0=0.924,$ and $V_0=61.3$ kV for the second case. The values of α for the two cases are 1.442 and 1.588, respectively. To compare the bandwidth at nearly equal efficiencies ($\sim 20\%$), we choose an interaction length $L_z=50L_x$ for the higher-energy beam and $L_z=40L_x$ for the lower-energy beam. The two cases have nearly equal bandwidths of $\Delta\omega/\omega_0=32.6\%$ and $31.4\%,$ respectively. The actual frequency range ($\Delta\omega=0.56\omega_{cut}$) for the first case is larger than that ($\Delta\omega=0.48\omega_{cut}$) for the second case. The center frequency ω_0 is also higher for the first case. The slope of the $\omega-k_z$ curves is larger at smaller ϵ and the interaction occurs over a wider frequency range for the same spread in $k_z.$

The beam temperature effects on the instantaneous bandwidth are shown in η versus f curves in Figs. 8(a) and 8(b) for two interaction lengths $L_z=50L_x$ and $L_z=60L_x.$ In these figures we use $\epsilon=10\epsilon_0, \beta_z=0.3, \bar{\Omega}_0=1.122,$ and $V_0=90$ kV. For $L_z=50L_x,$ the peak efficiency η_p decreases rapidly from 20.8% to 10.8% as $\Delta v_z/v_z$ increases from 0 to 2% but the bandwidth decreases by a small amount from 32% to 29%. For the same increase in $\Delta v_z/v_z,$ the bandwidth increases from

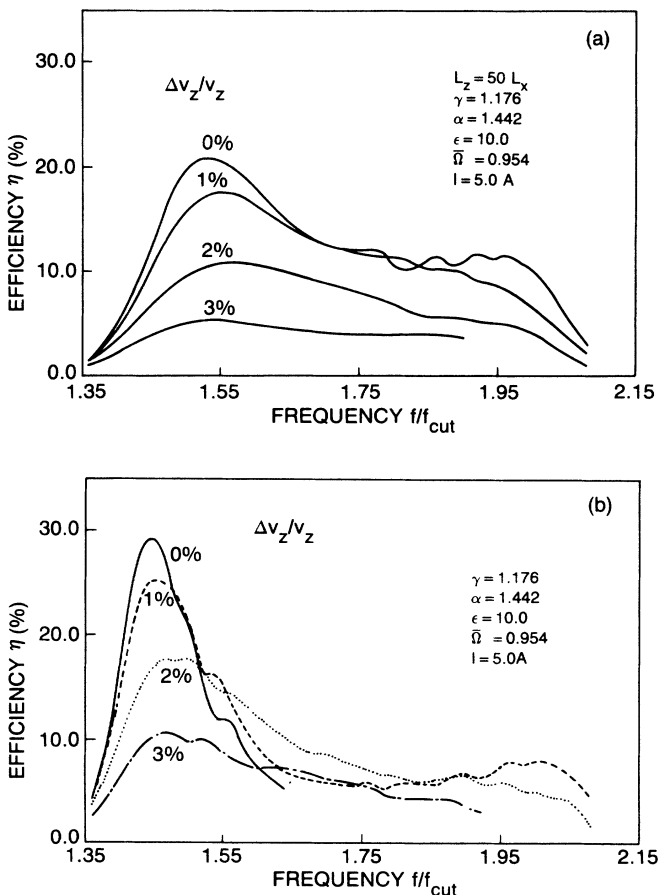


FIG. 8. Efficiency vs frequency for different values $\Delta v_z/v_z=0, 0.01,$ and 0.03 at (a) interaction length $L_z=50L_x$ and (b) $L_z=60L_x.$ Other parameters are $\epsilon=10\epsilon_0, \beta_z=0.3, \alpha=1.442, \bar{\Omega}_0=\gamma\bar{\Omega}=1.122,$ and $V_0=90$ kV.

9% to 19% when the interaction length is $L_z = 60L_x$. The peak efficiency, as usual, decreases from 29.2% to 17.6%.

IV. CONCLUSIONS

We have developed a 3D nonlinear theory of a slow-wave cyclotron amplifier in which an electron beam is guided in helical trajectories by a uniform magnetic field inside a dielectrically lined waveguide. The gain, bandwidth, and efficiency can be accurately calculated from the resulting numerical code. The rectangular waveguide configuration is better than the cylindrical configuration as a slow-wave cyclotron amplifier. The modes are orthogonal in the rectangular waveguide and the lowest mode is TE in character. The modes in the cylindrical configuration, on the other hand, are nonorthogonal and mode coupling is a problem. The relative dielectric constant of the layer in the waveguide should be in the range of 10 to 15 to obtain large instantaneous bandwidth and high efficiency with electron beam energy between 50 and 100 kV having $\alpha \approx 1.5$. The large signal bandwidth of the slow-wave cyclotron amplifier is comparable to that of the tapered fast-wave gyro-TWA but the efficiency is higher and the amplifier is free from spurious oscillations typical of the tapered circuits. Because the interaction in the slow-wave region occurs at higher values of k_z , the efficiency of the slow-wave cyclotron amplifier degrades more rapidly with increase in the beam temperature than the fast-wave gyrotrons. The bandwidth is not sensitive to the beam temperature and may increase as the beam temperature rises. One difficulty in the slow-wave experiment is that the beam has to be placed close to the dielectric layer for enhanced interaction and precautions should be taken to drain off the charges on the dielectric if some electrons reach the wall.

ACKNOWLEDGMENTS

The work was supported in part by the Office of Naval Research and in part by the Office of Naval Technology.

$$\mathbf{J}(\mathbf{r}, t) = -I_0 \int f_0(\mathbf{v}) d\mathbf{v} \frac{1}{A_b} \int_{A_b} \int_{-T/2}^{T/2} dx_0 dy_0 d(t_0) \sigma_T(x_0, y_0) \sigma_{\parallel}(t_0) \frac{v_{z0}}{\langle v_{z0} \rangle} \\ \times \frac{\mathbf{v}(\mathbf{x}, y, z, t)}{|v_z(\mathbf{x}, t, z; \mathbf{x}_0, t_0)|} \delta(x - x(\mathbf{x}_0, t_0, z)) \delta(y - y(\mathbf{x}_0, t_0, z)) \delta(t - t(\mathbf{x}_0, t_0, z)), \quad (\text{A4})$$

where $\mathbf{v}(\mathbf{x}, t, z; \mathbf{x}_0, t_0)$ is the velocity of an electron at axial position z with transverse position $\mathbf{x} = (x, y)$ which entered the waveguide at $z=0$ at time t_0 with transverse position $\mathbf{x}_0 = (x_0, y_0)$,

$$t(z; \mathbf{x}_0, y_0, t_0) = t_0 + \int_0^z \frac{dz'}{v_z(z'; \mathbf{x}_0, y_0, t_0)}$$

APPENDIX

Here we derive the set of the coupled nonlinear equations to describe the evolution of the electromagnetic field and the trajectories of an ensemble of electrons. From Eqs. (1), (6), and (12), we obtain

$$\sum_{n=1}^{\infty} \left[\left[\frac{d^2 F_n}{dz^2} + (k_{z0}^2 - k_z^2) \right] Z_{n0}(x) \cos \alpha_n + \frac{1}{F_n} \frac{d}{dz} (k_z F_n) Z_{n0}(x) \sin \alpha_n \right] \hat{\mathbf{e}}_y = \mu_0 \frac{\partial \mathbf{J}}{\partial t}, \quad (\text{A1})$$

where k_{z0} and k_z are defined in Eqs. (6) and (15), respectively. The subscript n has been suppressed in k_{z0} and k_z for clarity. Multiply both sides of Eq. (A1) by $\hat{\mathbf{e}}_y Z_{n0}(x) \cos \alpha_n$, integrate over the cross section of the waveguide, and average over a wave period. After using the orthogonal property of the functions $Z_{n0}(x)$ [Eq. (8)] and the cancellation of the end terms in the partial time integration due to the quasistatic assumption, we obtain

$$\frac{d^2 F_n}{dz^2} + (k_{z0}^2 - k_z^2) F_n = - \frac{2\mu_0 \omega}{L_x^2 N_n} \int_0^{2\pi} d(\omega t) \frac{1}{2\pi} \\ \times \int_{A_b} dx dy \hat{\mathbf{e}}_y \cdot \mathbf{J}(\mathbf{r}, t) Z_{n0}(x) \sin \alpha_n. \quad (\text{A2})$$

Similarly, multiplying Eq. (A1) by $\hat{\mathbf{e}}_y Z_n(x) \sin \alpha_n$ and repeating the procedure as in Eq. (A2), we get

$$2k_z^{1/2} \frac{d}{dz} (k_z^{1/2} F_n) = \frac{2\mu_0 \omega}{L_x^2 N_n} \int_0^{2\pi} d(\omega t) \frac{1}{2\pi} \\ \times \int_{A_b} dx dy \hat{\mathbf{e}}_y \cdot \mathbf{J}(\mathbf{r}, t) Z_{n0}(x) \cos \alpha_n, \quad (\text{A3})$$

where A_b is the cross-sectional area of the beam. The current density²⁴ can be written as

and $T = L/v_{z0}$, L being the length of the interaction region. The electronic current is $I_0 = n_0 e \langle v_{z0} \rangle$ where n_0 is the average electron density and $\langle v_{z0} \rangle$ is the average value of v_{z0} , the axial velocity at $z=0$. The initial distribution of the electrons in cross section, phase, and velocity are described, respectively, by σ_T , σ_{\parallel} , and $f_0(\mathbf{v})$ subject to the normalization

$$\int f_0(\mathbf{v})d\mathbf{v} = 1, \quad (A5)$$

$$\frac{1}{A_b} \int_{A_b} \sigma_T(x_0, y_0) dx_0 dy_0 = 1,$$

$$\frac{1}{T} \int_{-T/2}^{T/2} \sigma_{\parallel}(t_0) dt_0 = 1.$$

On substitution of Eq. (A4) into Eqs. (A2) and (A3), the integrations over x , y , and t are transferred to an integration over the initial distributions and using the expressions for \mathbf{r} and \mathbf{v} from Eqs. (18)–(20), we obtain

$$\frac{d^2 F_n}{dz^2} + (k_{z0}^2 - k_z^2) F_n$$

$$= - \frac{2eI_0}{\epsilon_0 m_0 c^3} \frac{\omega}{cL_x N_n}$$

$$\times \left\langle \frac{v_{z0}}{\langle v_{z0} \rangle} \frac{v_T}{|v_z|} Z_{n0}(x) \cos\Psi \sin\alpha_n \right\rangle, \quad (A6)$$

$$2k_z^{1/2} \frac{d}{dz} (k_z^{1/2} F_n)$$

$$= \frac{2eI_0}{\epsilon_0 m_0 c^3} \frac{\omega}{cL_x N_n}$$

$$\times \left\langle \frac{v_{z0}}{\langle v_{z0} \rangle} \frac{v_T}{|v_z|} Z_{n0}(x) \cos\Psi \cos\alpha_n \right\rangle, \quad (A7)$$

where $\alpha_n = \omega(t - t_0) - \xi + \Psi_0$, $\Psi_0 = \omega t_0$ and the symbol $\langle O \rangle$ defines an average of the variable O over the initial electron distribution function as

$$\langle O \rangle = \int f_0(\mathbf{v}) d\mathbf{v} \frac{1}{2\pi A_b}$$

$$\times \int_{A_b} O \sigma_T(R_0, \Theta_0) \sigma_{\parallel}(\Psi_0) dR_0 d\Theta_0 d\Psi_0, \quad (A8)$$

where R_0, Θ_0 are the polar coordinates corresponding to x_0, y_0 . Since the wave functions $Z_{n0}(x)$ in the region $-d < x < d$ where the beam propagates are of the form

$$\cosh(\kappa_n x) = \cosh[\kappa_n (X_0 + r_L \cos\Psi)] \quad (\text{for even modes})$$

or

$$\sinh(\kappa_n x) = \sinh[\kappa_n (X_0 + r_L \cos\Psi)] \quad (\text{for odd modes}),$$

these functions can be expanded²⁵ in a Fourier series of $\cos(s\Psi)$ whose coefficients are the modified Bessel functions $I_s(\kappa_n X_0)$ of the first kind. The product of the trigonometric functions $\cos(s\Psi)$, $\cos\Psi$, and $\cos\alpha_n$ or $\sin\alpha_n$ can be converted to sums whose arguments vary as $\cos(\alpha_n \pm s\Psi)$ or $\sin(\alpha_n \pm s\Psi)$ and the following identities are obtained for the even modes:

$$Z_{n0}(x) \sin\alpha_n \cos\Psi = \Theta_n \cosh(\kappa_n X_0) \sum_{s=1, \text{odd}}^{\infty} I'_s(\kappa_n r_L) [\sin(\alpha_n - s\Psi) + \sin(\alpha_n + s\Psi)]$$

$$- \Theta_n \sinh(\kappa_n X_0) \sum_{s=2, \text{even}}^{\infty} I'_s(\kappa_n r_L) [\sin(\alpha_n - s\Psi) + \sin(\alpha_n + s\Psi)], \quad (A9)$$

$$Z_{n0}(x) \cos\alpha_n \cos\Psi = \Theta_n \cosh(\kappa_n X_0) \sum_{s=1, \text{odd}}^{\infty} I'_s(\kappa_n r_L) [\cos(\alpha_n - s\Psi) + \cos(\alpha_n + s\Psi)]$$

$$- \Theta_n \sinh(\kappa_n X_0) \sum_{s=2, \text{even}}^{\infty} I'_s(\kappa_n r_L) [\cos(\alpha_n - s\Psi) + \cos(\alpha_n + s\Psi)], \quad (A10)$$

where $I'_s = dI_s(a)/da$ and the factor Θ_n is defined in Eq. (25). The results for the odd symmetry modes may be obtained by the following replacement in Eqs. (A9) and (A10):

$$\cosh(\kappa_n X_0) \rightarrow \sinh(\kappa_n X_0)$$

and

$$-\sinh(\kappa_n X_0) \rightarrow \cosh(\kappa_n X_0).$$

On substituting Eqs. (A9) and (A10) in Eqs. (A6) and (A7), it is seen that the average over the initial phase Ψ_0 for a beam with uniform distribution [i.e., $\sigma_{\parallel}(\Psi_0) = 1$ in the range $0 \leq \Psi_0 \leq 2\pi$] will be vanishingly small except for the resonant sth cyclotron harmonic for which $\Phi = \omega t - \xi - s\Psi$ is very small. Furthermore, all factors in the integrands of Eqs. (A6) and (A7) except $\sinh(\kappa_n X_0)$ or $\cosh(\kappa_n X_0)$ are insensitive to variation in Θ_0 . If the ini-

tial cross-sectional distribution $\sigma_T(R_0, \Theta_0)$ is, also, independent of Θ_0 , then

$$\int_0^{2\pi} \sinh(\kappa_n X_0) d\Theta_0 = 0$$

and

$$\int_0^{2\pi} \cosh(\kappa_n X_0) d\Theta_0 = I_0(\kappa_n R_0).$$

The terms in $\sinh(\kappa_n X_0)$ from Eqs. (A9) and (A10) vanish when averaged over the initial distribution and we obtain the selection rule that the odd cyclotron harmonics couple to the even symmetry waveguide modes and vice versa. Hence, considering the interaction with a single resonant cyclotron harmonic, we obtain from Eqs. (A6)–(A10) the following equations for the wave amplitude and the wave vector:

$$\begin{aligned} & \frac{d^2 F_n}{dz^2} + (k_{z0}^2 - k_z^2) F_n \\ &= - \frac{2eI_0}{\epsilon_0 m_0 c^3} \frac{\omega \Theta_n}{c L_x N_n} \\ & \quad \times \left\langle \frac{v_{z0}}{\langle v_{z0} \rangle} \frac{v_T}{|v_z|} I'_s(\kappa_n r_L) \cosh(\kappa_n X_0) \sin \Phi \right\rangle, \end{aligned} \quad (\text{A11})$$

$$\begin{aligned} & 2k_z^{1/2} \frac{d}{dz} (k_z^{1/2} F_n) \\ &= \frac{2eI_0}{\epsilon_0 m_0 c^3} \frac{\omega \Theta_n}{c L_x N_n} \\ & \quad \times \left\langle \frac{v_{z0}}{\langle v_{z0} \rangle} \frac{v_T}{|v_z|} I'_s(\kappa_n r_L) \cosh(\kappa_n X_0) \cos \Phi \right\rangle, \end{aligned} \quad (\text{A12})$$

where $\Phi = \omega t - \xi + s\Psi$ with s odd for even modes and s even for odd modes.

The equations of motion of the electrons in their helical trajectories can be derived from Eqs. (2), (12), (13), (18), and (19). Thus

$$\begin{aligned} \frac{d}{dt}(\gamma v_T) &= - \frac{c^2}{L_x} \sum_n \left[\left[1 - \frac{k_z v_z}{\omega} \right] F_n \cos \alpha_n \right. \\ & \quad \left. + \frac{v_z}{\omega} \frac{dF_n}{dz} \sin \alpha_n \right] Z_{n0}(x) \cos \Psi, \end{aligned} \quad (\text{A13})$$

$$\begin{aligned} \frac{d}{dt}(\gamma v_z) &= \frac{c^2}{L_x} \sum_n \frac{v_T}{\omega} \left[\frac{dF_n}{dz} \sin \alpha_n \right. \\ & \quad \left. - k_z F_n \cos \alpha_n \right] Z_{n0}(x) \cos \Psi, \end{aligned} \quad (\text{A14})$$

$$\begin{aligned} \frac{d\Psi}{dt} - \frac{\Omega_0}{\gamma} &= \frac{c^2}{\gamma v_T L_x} \sum_n \left[\left[1 - \frac{k_z v_z}{\omega} \right] F_n \cos \alpha_n \right. \\ & \quad \left. + \frac{v_z}{\omega} \frac{dF_n}{dz} \sin \alpha_n \right] Z_{n0}(x) \sin \Psi \\ & \quad - \frac{c^2}{\omega L_x} \sum_n \frac{dZ_{n0}(\kappa_n x)}{dx} F_n \sin \alpha_n. \end{aligned} \quad (\text{A15})$$

As in Eqs. (A9) and (A10), the various combinations of

$Z_{n0}(x)$, $\cos \Psi$, $\sin \Psi$, $\sin \alpha_n$, and $\cos \alpha_n$ can be expanded in a Fourier series of $\sin(\alpha_n \pm s\Psi)$ and $\cos(\alpha_n \pm s\Psi)$ in which the coefficients are either $I'_s(\kappa_n r_L)$ or $sI_s(\kappa_n r_L)/\kappa_n r_L$. Again, retaining only the resonant s th cyclotron harmonic term for which the phase $\Phi = \alpha_n - s\Psi$ is slowly varying, we get

$$\begin{aligned} & \frac{d}{dt}(\gamma v_T) \\ &= - \frac{c^2}{L_x} \sum_n \left[\left[1 - \frac{k_z v_z}{\omega} \right] F_n \cos \Phi + \frac{v_z}{\omega} \frac{dF_n}{dz} \sin \Phi \right] \\ & \quad \times \Theta_n I'_s(\kappa_n r_L) \cosh(\kappa_n X_0), \end{aligned} \quad (\text{A16})$$

$$\begin{aligned} \frac{d}{dt}(\gamma v_z) &= \frac{c^2}{L_x} \sum_n \frac{v_T}{\omega} \left[\frac{dF_n}{dz} \sin \Phi - k_z F_n \cos \Phi \right] \\ & \quad \times \Theta_n I'_s(\kappa_n r_L) \cosh(\kappa_n X_0), \end{aligned} \quad (\text{A17})$$

and

$$\begin{aligned} \frac{d\Psi}{dt} - \frac{\Omega_0}{\gamma} &= \frac{c^2}{\gamma v_T L_x} \sum_n \left[\left[1 - \frac{k_z v_z}{\omega} + \frac{\kappa_n^2 r_L^2 \Omega_0}{s \gamma \omega} \right] F_n \cos \Phi \right. \\ & \quad \left. - \frac{v_z}{\omega} \frac{dF_n}{dz} \sin \Phi \right] \\ & \quad \times \Theta_n \frac{s I_s(\kappa_n r_L)}{\kappa_n r_L} \cosh(\kappa_n X_0). \end{aligned} \quad (\text{A18})$$

As mentioned before, odd and even cyclotron harmonic numbers appear in Eqs. (A16)–(A18) for interaction with the even and odd wave modes.

The equations of motion for the guiding center coordinates in the slow-time-scale formulation can similarly be obtained from Eqs. (12), (13), and (18)–(22) and we get

$$\begin{aligned} \frac{dX_0}{dt} &= \sum_n \frac{c^2 \Theta_n I_s(\kappa_n r_L)}{L_x \Omega_0} \sinh(\kappa_n X_0) \\ & \quad \times \left[\frac{\omega - k_z v_z - s \Omega}{\omega} F_n \cos \Phi \right. \\ & \quad \left. + \frac{v_z}{\omega} \frac{dF_n}{dz} \sin \Phi \right], \end{aligned} \quad (\text{A19})$$

$$\frac{dY_0}{dt} = \sum_n \Theta_n I'_s(\kappa_n r_L) \sinh(\kappa_n X_0) \frac{c^2 \kappa_n r_L}{\gamma L_x \omega} F_n \sin \Phi. \quad (\text{A20})$$

¹V. A. Flyagin, A. V. Gaponov, M. I. Petelin, and V. K. Yulpatov, IEEE Trans. Microwave Theory Tech. **MTT-25**, 514 (1977).

²J. L. Hirshfield and V. L. Granatstein, IEEE Trans. Microwave Theory Tech. **MTT-25**, 522 (1977)

³S. Ono, K. Tsutaki, and T. Kageyama, Int. J. Electron. **56**, 507 (1984).

⁴E. S. Weibel, Phys. Rev. Lett. **2**, 83 (1959).

⁵P. Vitello, IEEE Trans. Microwave Theory Tech. **MTT-32**, 917 (1984).

⁶A. K. Ganguly and S. Ahn, Int. J. Electron. **65**, 597 (1988).

⁷K. R. Chu and J. L. Hirshfield, Phys. Fluids **21**, 461 (1978).

⁸A. K. Ganguly and S. Ahn, Int. J. Electron. **53**, 641 (1983).

⁹L. R. Barnett, L. H. Chang, H. Y. Chen, K. R. Chu, W. K. Lau, and C. C. Tu, Phys. Rev. Lett. **63**, 1062 (1989).

¹⁰L. Barnett, D. Dialetis, Y. Y. Lau, and K. R. Chu, *Interna-*

- tional Electron Devices Meeting 83 Technical Digest* (IEEE, New York, 1983), pp. 280–283.
- ¹¹K. R. Chu, A. K. Ganguly, V. L. Granatstein, J. L. Hirshfield, S. Y. Park, and J. M. Baird, *Int. J. Electron.* **51**, 493 (1981).
- ¹²A. K. Ganguly and K. R. Chu, Naval Research Laboratory Memorandum Report No. 4215, 1980 (unpublished).
- ¹³R. F. Harrington, *Time Harmonic Electromagnetic Fields* (McGraw-Hill, New York, 1961), p. 158.
- ¹⁴G. N. Rapoport, A. K. Nematik, and V. A. Zhurakhovskiy, *Radio Eng. Electron. Phys. (USSR)* **12**, 587 (1967).
- ¹⁵A. W. Fliflet, M. E. Read, K. R. Chu, and R. Seeley, *Int. J. Electron.* **53**, 505 (1982).
- ¹⁶A. K. Ganguly and H. P. Freund, *Phys. Rev. A* **32**, 2275 (1985).
- ¹⁷P. Sprangle, A. Ting, and C. M. Tang, *Phys. Rev. Lett.* **59**, 202 (1987), *Phys. Rev. A* **36**, 2773 (1987).
- ¹⁸A. K. Ganguly, H. P. Freund, and S. Ahn, *Phys. Rev. A* **36**, 2199 (1987).
- ¹⁹A. M. Woodward, *Wireless Eng.* **24**, 192 (1947).
- ²⁰H. Guo, L. Chen, H. Keren, and J. L. Hirshfield, *Phys. Rev. Lett.* **49**, 730 (1982).
- ²¹*Handbook of Tables for Applied Engineering Science*, edited by R. E. Bolz and G. L. Tuve (CRC, Cleveland, 1973), p. 262.
- ²²K. C. Gupta, R. Garg, and I. J. Bahl, *Microstrip Lines and Slotlines* (Artech, Norwood, MA, 1979), p. 73.
- ²³R. R. Bonetti and A. E. Williams, *Institute of Electrical and Electronics Engineers Microwave Theory and Techniques Symposium, Dallas, 1990* (Institute of Electrical and Electronics Engineers, New York, 1990), p. 273.
- ²⁴P. Sprangle, C. M. Tang, and W. Manheimer, *Phys. Rev. A* **21**, 302 (1980).
- ²⁵*Handbook of Mathematical Functions*, Natl. Bur. Stand. Appl. Math. Ser. No. 55, edited by M. Abramowitz and I. Stegun (U.S. GPO, Washington, D.C., 1964), p. 376.